Title
Springtime extreme moisture transport into the Arctic and its impact on sea ice concentration

Journal
Journal of Geophysical Research: Atmospheres, 122(10)

ISSN
2169-897X

Authors
Yang, Wenchang
Magnusdottir, Gudrun

Publication Date
2017-05-27

DOI
10.1002/2016jd026324

AGU PUBLICATIONS

JGR

Journal of Geophysical Research: Atmospheres

RESEARCH ARTICLE
10.1002/2016JD026324

Special Section:
The Arctic: An AGU Joint Special Collection

Springtime extreme moisture transport into the Arctic and its impact on sea ice concentration

Wenchang Yang[1] and **Gudrun Magnusdottir**[1]

[1]Department of Earth System Science, University of California, Irvine, California, USA

Key Points:
- Springtime extreme moisture transport into the Arctic is dominant over Atlantic longitudes
- Extreme moisture transport reduces sea ice concentration and increases surface air temperature over the Greenland-Barents-Kara Seas
- Over 60% of the extreme moisture transport days are associated with the Atlantic blocking weather regime

Supporting Information:
- Supporting Information S1

Correspondence to:
W. Yang,
yang.wenchang@uci.edu

Citation:
Yang, W., and G. Magnusdottir (2017), Springtime extreme moisture transport into the Arctic and its impact on sea ice concentration, *J. Geophys. Res. Atmos.*, *122*, 5316–5329, doi:10.1002/2016JD026324.

Received 2 DEC 2016
Accepted 5 MAY 2017
Accepted article online 12 MAY 2017
Published online 30 MAY 2017

Abstract Recent studies suggest that springtime moisture transport into the Arctic can initiate sea ice melt that extends to a large area in the following summer and fall, which can help explain Arctic sea ice interannual variability. Yet the impact from an individual moisture transport event, especially the extreme ones, is unclear on synoptic to intraseasonal time scales and this is the focus of the current study. Springtime extreme moisture transport into the Arctic from a daily data set is found to be dominant over Atlantic longitudes. Lag composite analysis shows that these extreme events are accompanied by a substantial sea ice concentration reduction over the Greenland-Barents-Kara Seas that lasts around a week. Surface air temperature also becomes anomalously high over these seas and cold to the west of Greenland as well as over the interior Eurasian continent. The blocking weather regime over the North Atlantic is mainly responsible for the extreme moisture transport, occupying more than 60% of the total extreme days, while the negative North Atlantic Oscillation regime is hardly observed at all during the extreme transport days. These extreme moisture transport events appear to be preceded by eastward propagating large-scale tropical convective forcing by as long as 2 weeks but with great uncertainty due to lack of statistical significance.

1. Introduction

Over the recent decades, the Arctic has warmed twice as fast as the rest of the Northern Hemisphere [*Winton*, 2006; *Serreze and Barry*, 2011; *Pithan and Mauritsen*, 2014; *Walsh*, 2014], and this is referred to as Arctic Amplification (AA). Contributing to the AA is the rapid decrease in Arctic sea ice concentration (SIC). SIC has decreased especially in September when the SIC reaches its annual minimum, although the background seasonal cycle is still dominating (Figure 1). The rapid decline of Arctic SIC, often viewed as a direct or indirect indicator of global warming, raises broad concerns from both the scientific community and the general public.

Arctic SIC exhibits substantial interannual variability that is superimposed on the long-term SIC decline (Figure 1c), and this is also an important and interesting scientific issue. External forcings of this short-term fluctuations could be from either oceanic [*Zhang et al.*, 1999; *Årthun et al.*, 2012] or atmospheric circulations [*Ogi and Wallace*, 2007; *Rigor et al.*, 2002] or both. In particular, the atmospheric circulation can impact the SIC either dynamically through the change of surface winds or thermodynamically through the associated heat and moisture fluxes into the Arctic [*Tjernström et al.*, 2015; *Ding et al.*, 2017]. Of the two types of fluxes, the moisture flux is found to be more important than the sensible heat flux due to the greenhouse effect [*Koenigk et al.*, 2013; *Graversen and Burtu*, 2016]. Several other studies have also concluded that the moisture flux transported into the Arctic can induce anomalous downward longwave radiation at the surface [*Woods et al.*, 2013; *Park et al.*, 2015a; *Mortin et al.*, 2016; *Woods and Caballero*, 2016]. Therefore, it is a sensible hypothesis that anomalously high moisture transport into the Arctic, which is usually accompanied by intense surface winds and a burst of moisture content and warming within the Arctic atmospheric column, will lead to a decreased Arctic SIC. Indeed, recent studies show that in years when there is low Arctic sea ice concentration in summer and fall, there is increased moisture transport into the Arctic in the preceding winter and spring [*Kapsch et al.*, 2013; *Park et al.*, 2015b].

Since the seasonal mean moisture transport in the extratropics is ultimately the result of integral contributions from individual transport events that are associated with synoptic weather systems, an interesting question is how does an individual moisture transport event impact Arctic sea ice as well as atmospheric conditions near the surface on synoptic to intraseasonal time scales? In particular, what are the characteristics of the impacts from the extreme moisture transport event? In this study, we will use daily reanalysis data to find extreme

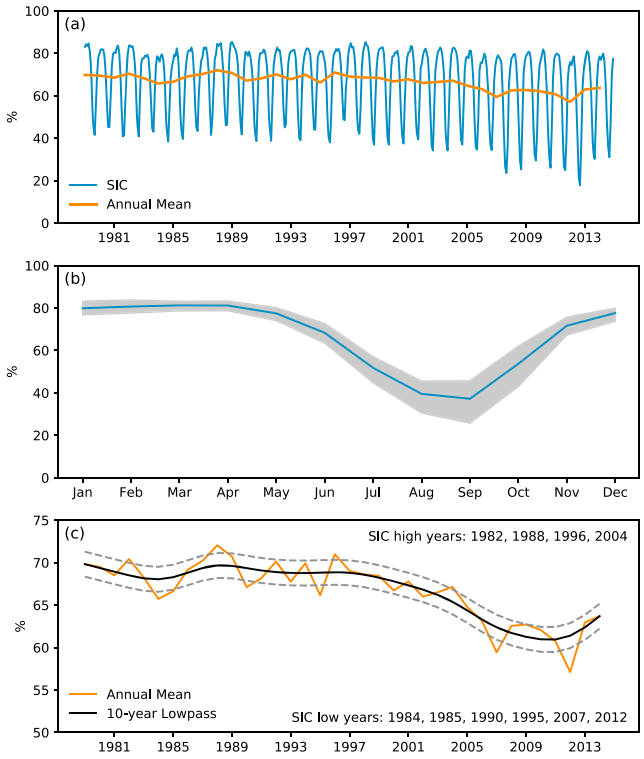

Figure 1. Sea ice concentration (SIC) averaged over the Arctic region (ocean area north of 70°N). (a) Monthly (blue) and annual (orange) mean, (b) seasonal cycle: multiyear mean (blue line) as well as its range between the 90th and 10th percentiles (gray shaded), and (c) annual mean (orange solid line) and 10 year low-pass filtered (black solid line), while dashed lines are one standard deviation (of the high-frequency component) above and below the low-frequency component.

moisture transport events into the Arctic and examine how these extreme events impact Arctic SIC, surface air temperature, and the surface energy flux. We will also investigate what weather regimes are associated with these extreme events and if there are any precursors from tropical convective activity as has been suggested in some recent studies [e.g., *Cassou*, 2008; *Park et al.*, 2015a]. Our study differs from *Park et al.* [2015a] in that we define the extreme events directly in terms of the moisture transport into the Arctic rather than the surface downward longwave radiation. Our study is also different from *Woods et al.* [2013] and *Park et al.* [2015a] in that we focus on the spring season, while their interest is in the winter season. Previous studies suggested the importance of moisture transport in winter [*Park et al.*, 2015a; *Persson et al.*, 2016]. The focus on spring in this study is inspired by the work of *Kapsch et al.* [2013] as well as our own analysis showing that spring moisture transport is more closely related to the Arctic annual mean SIC. Finally, we will concentrate on the moisture transport through the Atlantic channel since the transport is dominant along these longitudes evidenced by *Woods et al.* [2013] and our own analysis.

The paper is organized as follows. Section 2 describes the data and methods used in this study. Section 3 shows results, first as Arctic SIC interannual variability. Next, we obtain extreme events in terms of moisture transport into the Arctic and use these extreme events to perform lag composite analysis on SIC, surface air temperature, and surface energy flux. The last part in section 3 examines the weather regimes associated with the extreme moisture transport and possible precursors from tropical convective activity. Summary and concluding remarks will be presented in section 4.

2. Data and Methods

2.1. Data

For both monthly and daily Arctic sea ice concentration, we use data from the U.S. National Snow and Ice Data Center using the NASA Team algorithm [*Swift and Cavalieri*, 1985]. Sea ice concentration (SIC) in this data set is estimated from passive microwave brightness temperatures. While the original data are on a polar

stereographic grid with a spatial resolution of 25 km × 25 km, we regridded them onto a 1° × 1° longitude-latitude grid. The SIC data used in this study, both daily and monthly, range from the year 1979 to 2014. Since the SIC data are only available every 2 days before 1989, the daily SIC data during 1979–1988 are obtained by linear interpolation in time.

We use the European Centre for Medium-Range Weather Forecasts interim Re-Analysis (ERA-Interim) [*Dee et al.*, 2011] for surface air temperature, surface downward longwave (infrared) radiation, 500 hPa geopotential height (Z500), 200 hPa velocity potential (VP200), and vertically integrated moisture transport. The data set is available from 1979 to present, and the period of 1979–2014 is used in this study. The total horizontal wind field may be expressed as the sum of the rotational and the divergent part of the circulation. The gradient of the velocity potential is the divergent part of the horizontal wind. By continuity, centers of negative velocity potential in the tropical upper troposphere imply areas of active convection.

ERA-Interim reanalysis is usually considered to have the highest quality relative to other reanalysis data, especially over the Arctic region [*Jakobson et al.*, 2012], and this includes a better representation of mass fluxes including water vapor [*Graversen et al.*, 2011]. The vertically integrated moisture transport (Vlq**v**), which is immediately available from ERA-Interim, is defined as follows:

$$\mathrm{Vlq}\mathbf{v} = g^{-1}\int_{p_t}^{p_s} q\mathbf{v}\mathrm{d}p,$$

where **v** is the horizontal wind vector, q is specific humidity, g is the gravitational acceleration near the Earth surface, p_s is the surface air pressure, and p_t is the air pressure at the top of the atmospheric column. These data are available every 6 h, and their daily means are calculated and used in our analysis. We also interpolated all the re-analysis data onto a 2° × 2° longitude-latitude grid.

The daily Madden-Julian Oscillation (MJO) phase data used in this study are described in *Wheeler and Hendon* [2004] and can be obtained from http://www.bom.gov.au/climate/mjo. There are eight MJO phases, and each phase corresponds to a specific range of longitudes where there is active convection in the equatorial area. In general, the relationship between the MJO phase and the longitudes of active convection is phases 2 and 3 the Indian Ocean, phases 4 and 5 the Maritime Continent, phases 6 and 7 the western Pacific Ocean, and phases 8 and 1 the Western Hemisphere and Africa (see http://www.cpc.ncep.noaa.gov/products/precip/CWlink/MJO/mjo.shtml).

2.2. Methods

For each data set used in the composite analysis we subtract a 30 day running mean of the daily climatology to eliminate the seasonal cycle. We also eliminate the linear trend at each grid point for each calendar day of these data sets. The techniques of removing the smoothed seasonal cycle and the long-term trend are similar to the methods in *Yang and Magnusdottir* [2016]. To examine the variability of moisture transport into the Arctic, we construct a time series of zonal mean vertically integrated meridional moisture transport at 70°N (Vlqv70N):

$$\mathrm{Vlqv70N} = 360^{-1}\int_{0}^{360} \mathrm{Vlqv}|_{70\mathrm{N}}\mathrm{d}\lambda,$$

where λ is longitude, $\mathrm{Vlqv}|_{70\mathrm{N}}$ is the meridional component of the vertically integrated moisture transport (Vlq**v**) at 70°N. Similarly, we construct another time series, named "Atlantic-Vlqv70N," which is also the vertically integrated moisture flux but longitudinally averaged between 30°W and 30°E:

$$\mathrm{Atlantic\text{-}Vlqv70N} = 60^{-1}\int_{-30}^{30} \mathrm{Vlqv}|_{70\mathrm{N}}\mathrm{d}\lambda.$$

In this study, days with the top 15% daily values of Vlqv70N or Atlantic-Vlqv70N for a given season are defined as "extreme" days. An extreme event is defined as a sequence of consecutive extreme days preceded and followed by nonextreme days. An extreme event duration is defined as the number of days for the extreme event and the first day of an extreme event is defined as "lag day 0" in the lag composite analysis. In order to filter out noise of day-to-day fluctuations, a 5 day low-pass filter (which is a second-order forward-backward Butterworth low-pass filter) is applied to the composite data sets before the lag composite analysis is conducted.

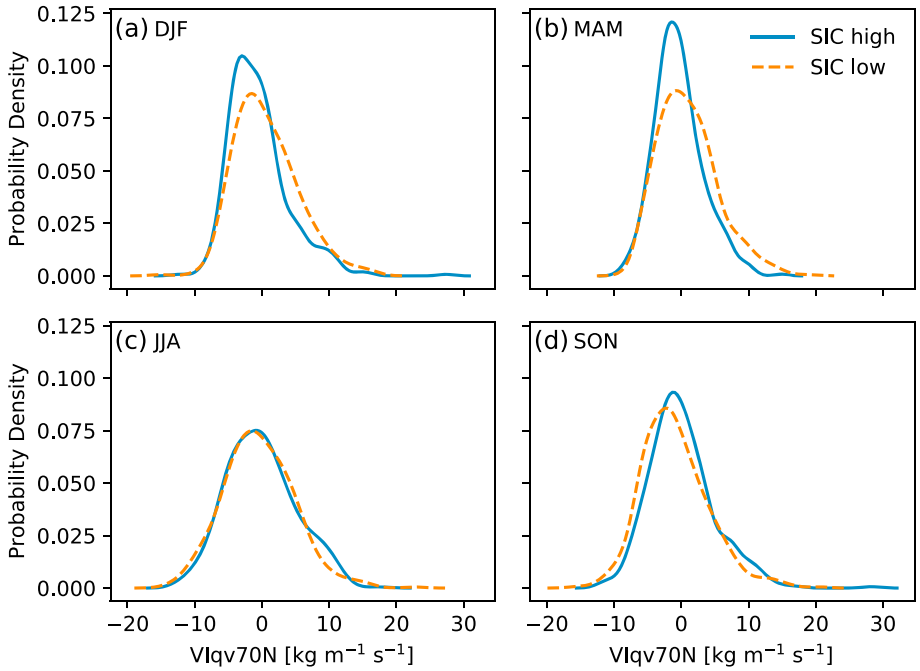

Figure 2. Probability density of vertically integrated meridional daily moisture flux anomaly zonally averaged at 70°N for SIC high (solid lines) and SIC low (dashed lines) years in the season (a) DJF, (b) MAM, (c) JJA, and (d) SON. Here the season DJF of a given year includes January and February of that year and the month of December before the given year. The anomaly is obtained by removing the seasonal cycle and multiyear linear trend at each calendar day at each grid point as described in section 2.2.

To identify daily weather regimes over the North Atlantic area, the k-means clustering method is applied to the daily Z500 anomalies over the areas of 90°W–60°E and 20°N–80°N including all seasons from 1979 to 2014. As stated before, the anomalies are obtained by removing the seasonal cycle as well as the multiyear trend at each calendar day and each grid point. The number of clusters is set as four to be consistent with previous studies [*Michelangeli et al.*, 1995; *Cassou*, 2008; *Peings and Magnusdottir*, 2014], which have shown that there are four typical weather regimes over this region: the North Atlantic Oscillation (NAO) Positive Polarity (NAO$^+$), NAO Negative Polarity (NAO$^-$), blocking, and Atlantic Ridge. The result of our analysis is shown in Figure S1 in the supporting information, and all the days are grouped into one of the four weather regimes in this study.

3. Results

3.1. SIC Variability

Before investigating the impact of extreme moisture transport into the Arctic, we first look at the Arctic SIC temporal variability. Figure 1a shows the SIC monthly (blue) and annual mean (green) time series averaged over the Arctic areas (north of 70°N). The monthly SIC shows a large seasonal cycle. Its seasonal maximum (usually occurs in January–April as shown in Figure 1b) can reach values of 80%, yet the seasonal minimum (generally in September as shown in Figure 1b) goes below 40% and even falls below 20% in 2012, a record SIC low year.

The seasonal cycle of the Arctic SIC also shows a long-term increasing trend in amplitude, primarily attributed to the decrease of the SIC seasonal minimum. The difference between the seasonal maximum and minimum increases from ~40% in the 1980s and 1990s to ~60% in recent years. In addition, the annual mean Arctic SIC has also been declining by approximately 10% since 1979 shown as the green line in Figure 1a. This is illustrated in detail in Figure 1c. While the long-term decline in the annual mean Arctic SIC is significant and raises alarm both with scientists and the general public, there are also substantial interannual fluctuations, which have attracted less attention. To obtain the Arctic SIC interannual variability, we first divide the annual mean time series into low (the black solid line in Figure 1c) and high-frequency components. Then we define the years when the annual mean SIC is one standard deviation (of the high-frequency component) above/below

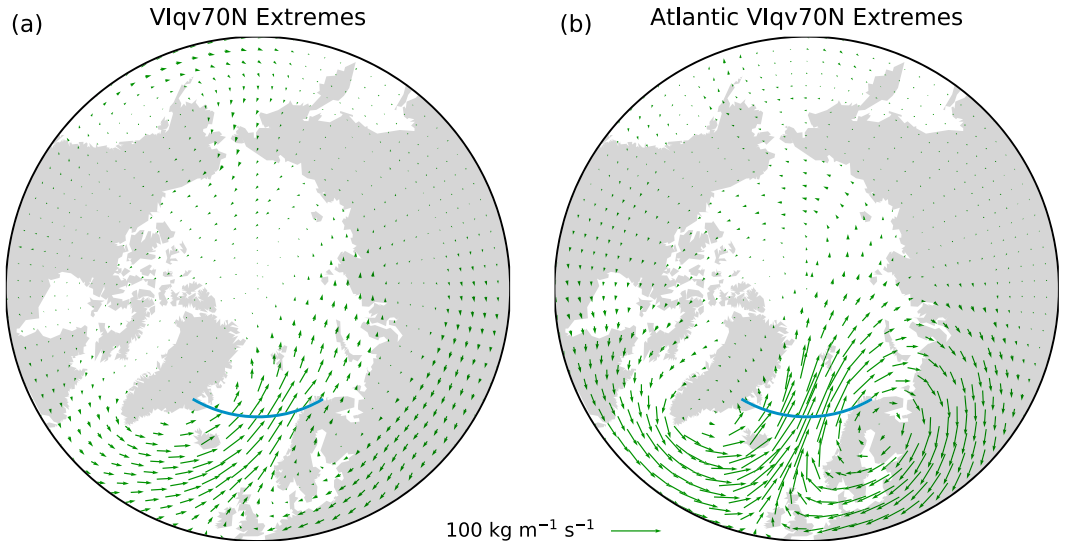

Figure 3. Composites of MAM vertically integrated moisture transport (VIq**v**) for extremes of (a) VIqv70N and (b) Atlantic-VIqv70N. The blue solid lines show the defined Atlantic longitude range 30°W–30°E at 70°N.

the low-frequency component as the SIC high/low years. This yields five SIC high years, i.e., year 1982, 1988, 1996, 2004, and 2013 and five SIC low years, i.e., year 1984, 1990, 1995, 2007, and 2012.

3.2. Moisture Transport Into the Arctic

Kapsch et al. [2013] showed that an increase in moisture transport into the Arctic in spring leads to an enhanced greenhouse effect that plays an important role in initiating the melt that becomes an extensive area of melt in September. Yet how the daily moisture transport probability distribution in the SIC low years differs from that in the SIC high years is unclear. Figure 2 shows the estimated probability density function (PDF) of the daily VIqv70N. The PDFs of SIC low years (dashed lines) are compared to those of SIC high years (solid lines) for each season. In SIC low years, both December–February (DJF) (Figure 2a) and March–May (MAM) (Figure 2b) moisture transports into the Arctic are enhanced, indicated by the rightward shift of the PDF profile. As a result, extreme transport occurs more frequently in the SIC low years. This is more apparent in the

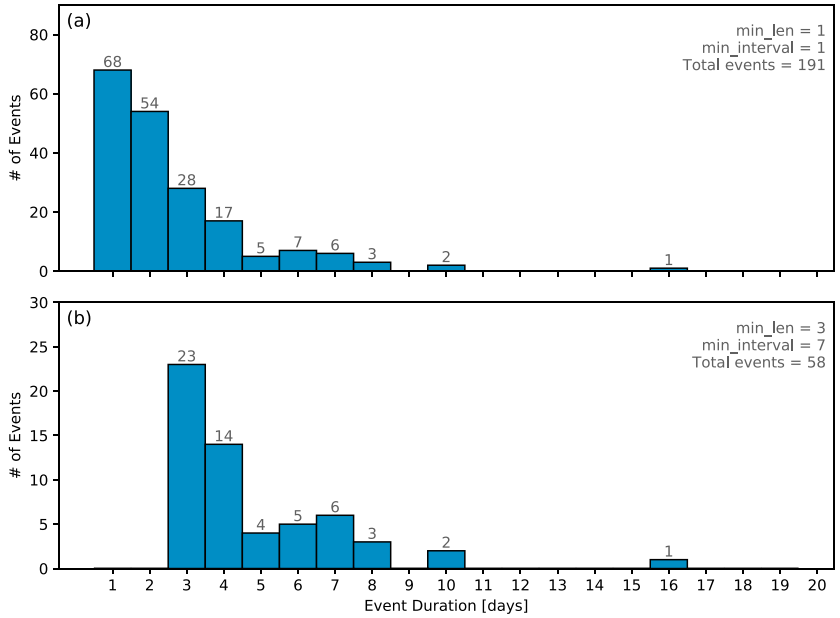

Figure 4. (a) Histogram of MAM Atlantic-VIqv70N extreme event durations. (b) Same as Figure 4a except that only events lasting for three or more days are selected and each event is at least 7 days away from other events.

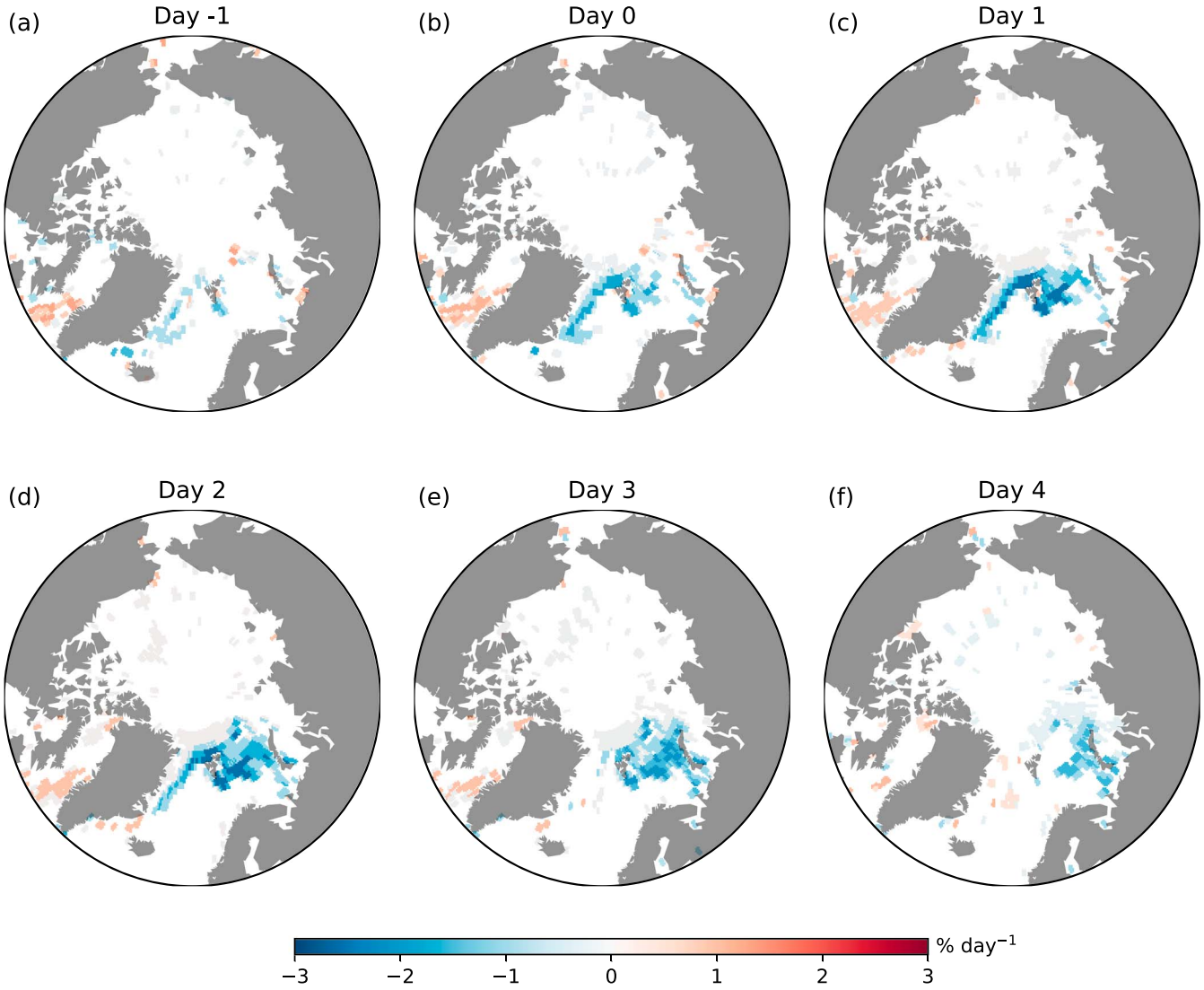

Figure 5. MAM composites of SIC tendency at lag day (a) −1, (b) 0, (c) 1, (d) 2, (e) 3, and (f) 4 for the Atlantic-VIqv70N extreme events. Day 0 is defined as the first day of the event. Shaded areas are significant at the 0.05 level by the two-sided Student's *t* test.

spring season and is consistent with previous studies [*Kapsch et al.*, 2013; *Park et al.*, 2015b]. However, this is not the case for June–August (JJA) (Figure 2c) or September–November (SON) (Figure 2d). There is little difference in VIqv70N PDF between the SIC high and low years in the JJA season and the PDF profile even shifts toward the left in the SON season. One possible explanation is that the anomalously low sea ice during SIC low years induces warmer and therefore more humid Arctic summer and autumn conditions which reduce the meridional humidity gradient and moisture transport.

Figure 3a shows a composite of MAM vertically integrated moisture transport (VIq**v**) for the extreme VIqv70N days. The poleward moisture transport into the Arctic is not evenly distributed in longitude; rather, it is concentrated in a narrow channel over the North Atlantic. Inspired by this feature, from now on we will focus on the moisture transport over the Atlantic sector. We adopt a new index of moisture transport into the Arctic, Atlantic-VIqv70N, which is the longitudinal average between 30°W and 30°E. The composite of the MAM VIq**v** is reconstructed by using the new index, and the result is shown in Figure 3b. Compared to Figure 3a, the composite moisture transport over the Atlantic is more apparent. The moisture transport also manifests a cyclonic flow pattern centered over Greenland and an anticyclonic flow pattern centered near the Scandinavia. These flow patterns can also be seen in Figure 3a but are not as clearly depicted.

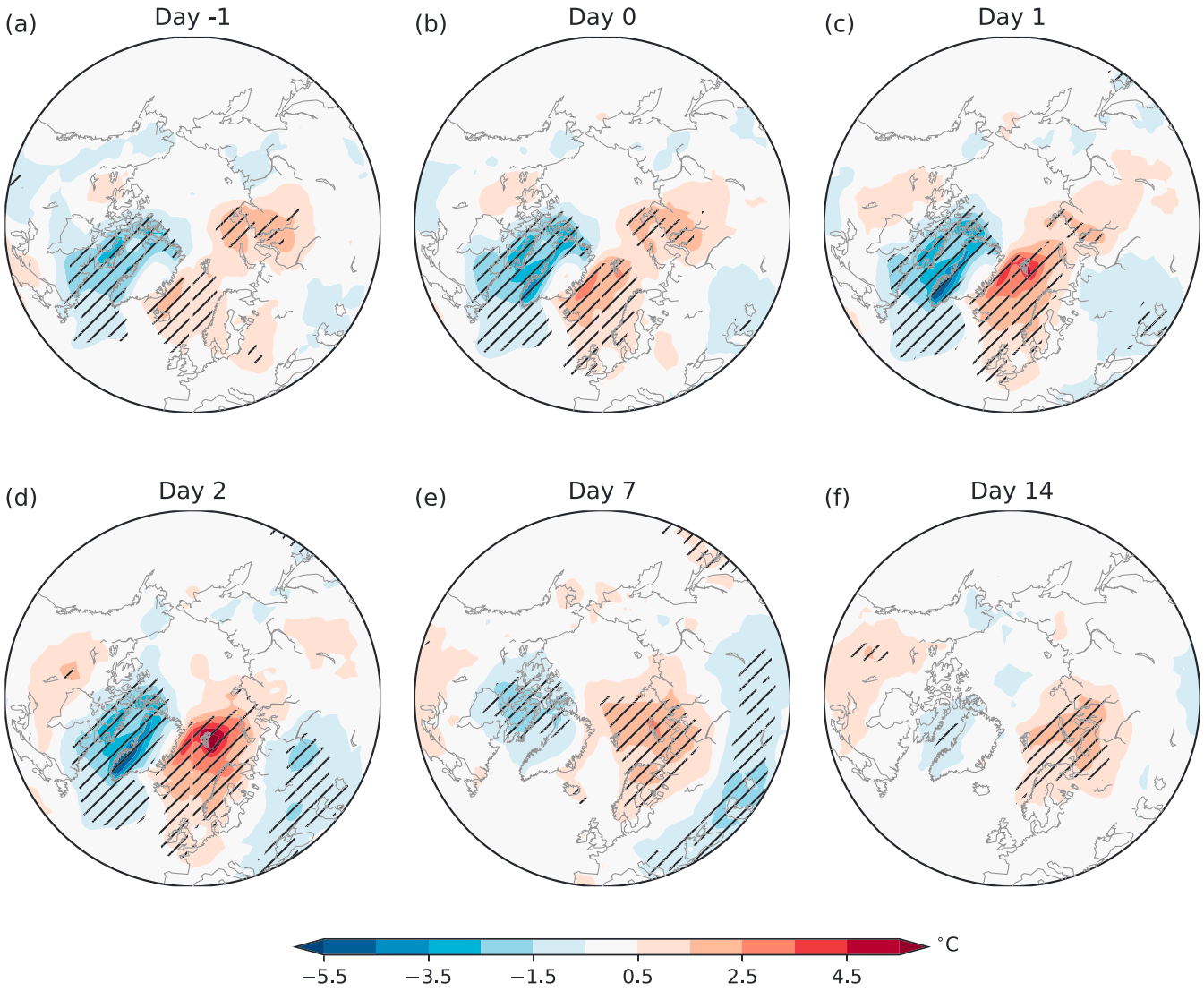

Figure 6. Same as Figure 5 except for the composites of surface air temperature. Hatched areas are significant at the 0.05 level by the two-sided Student's *t* test.

How long can each of the extreme Atlantic-VIqv70N events last? Figure 4 shows the histograms of the Atlantic-VIqv70N extreme events according to their duration. If the extreme event is loosely defined, i.e., the minimum duration is 1 day and the minimum gap between different events is also 1 day, the result is shown in Figure 4a. A large portion of events defined in this way are distributed on the "short" end of the duration, and the number of events decreases significantly as the event duration increases. As a matter of fact, almost two thirds of the total events last less than 3 days. In order to study the extreme events that are persistent and independent, we add two extra criteria to the definition of the events: (1) the minimum duration is 3 days and (2) the minimum gap between different events is 7 days. The first criterion ensures persistence of events, while the second one ensures their independence. The resulting histogram is shown in Figure 4b, which generally follows Figure 4a for duration greater than 2 days. This is caused by the additional requirement of event persistence and independence. From now on, we will use this definition to conduct lag composite analysis in the following sections.

3.3. Impact of Extreme Moisture Transport

Figure 5 shows the lag composites of daily SIC tendency for the Atlantic-VIqv70N extreme events. The SIC tendency (dSIC/d*t*) is approximated by the central difference of SIC along the time dimension, i.e., SIC tendency at day *i* is as follows:

$$\mathrm{dSIC}_i/\mathrm{d}t \approx (\mathrm{SIC}_{i+1} - \mathrm{SIC}_{i-1})/2.$$

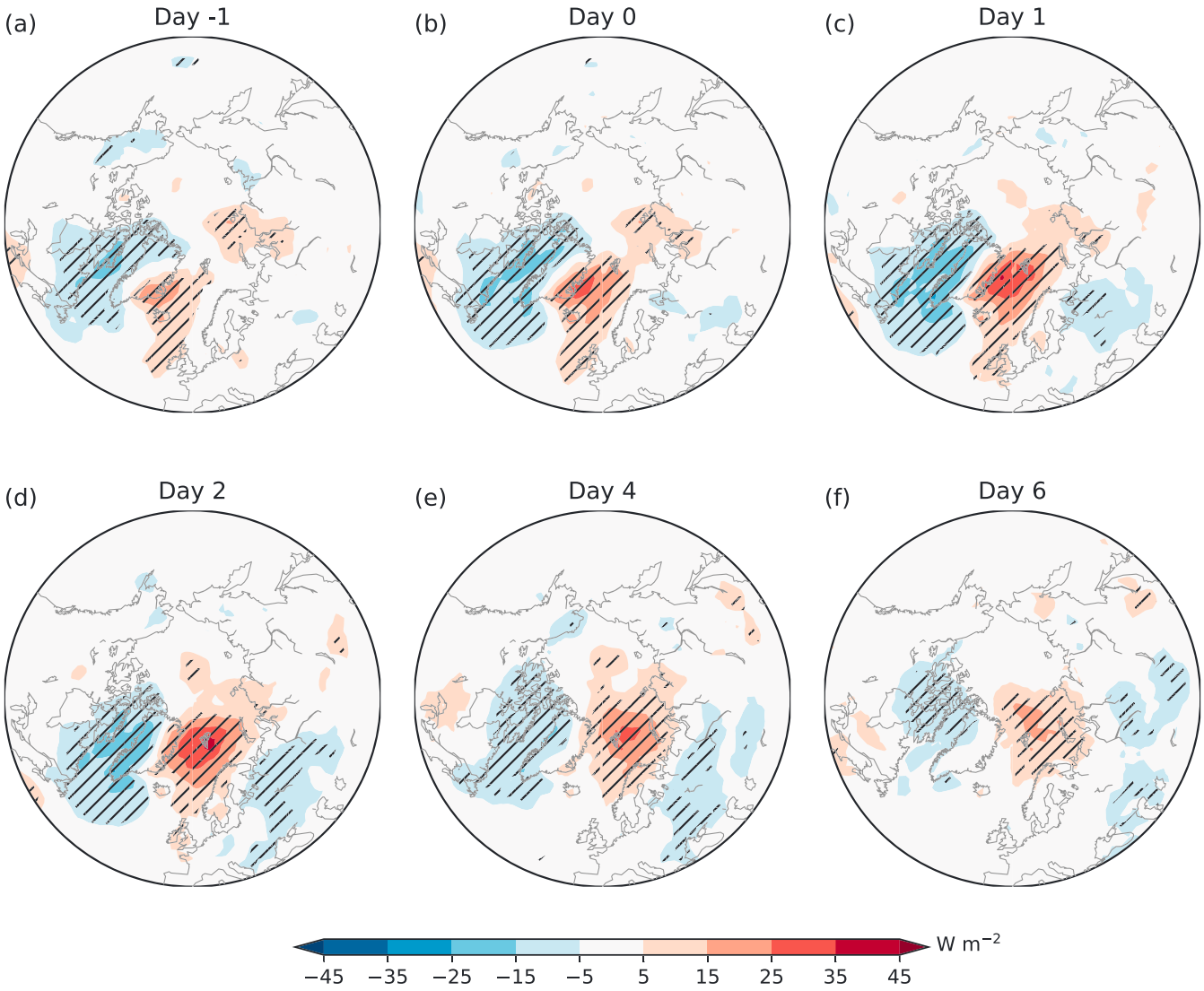

Figure 7. Same as Figure 6 except for the composites of surface downward longwave radiation.

Composites on day −1, 0, 1, 2, 3, and 4 are shown in Figures 5a–5f, respectively. The decrease in SIC starts as early as on lag day −1, appearing over the Greenland Sea along the east coast of Greenland. Some sporadic SIC reduction also occurs over the Barents Sea. At the same time, significant SIC enhancement appears to the southwest of Greenland, which indicates that some large-scale, organized weather phenomena may be responsible for the SIC tendency pattern around Greenland. On lag day 0 (Figure 5b), the SIC reduction-enhancement pattern intensifies and the SIC reduction also expands eastward to cover a large portion of the Barents Sea. This trend continues on lag day 1 (Figure 5c). On lag day 2 (Figure 5d), SIC reduction over the Greenland Sea is not apparent and the Barents Sea is now the center of SIC reduction. SIC tendency pattern continues to shift eastward to the Kara Sea and starts to weaken on lag day 3 (Figure 5e) and further weakens on lag day 4 (Figure 5f). Overall, extreme moisture transport through the Atlantic channel is shown to have significant impact on the SIC variability over the Greenland-Barents-Kara Seas and the impact has a time scale of around a week. Further analysis shows that it generally takes around 1 month for the negative SIC anomaly to recover to the level before the extreme event (Figure S2).

Figure 6 shows the impact of extreme moisture transport on the surface air temperature. The anomalously warm and cool patterns are generally consistent with the SIC tendency patterns in Figure 5. For example, the surface air is warmer to the east of Greenland but colder to the west and southwest of Greenland, consistent with the SIC reduction and increase in the corresponding seas. Furthermore, starting from lag day 2

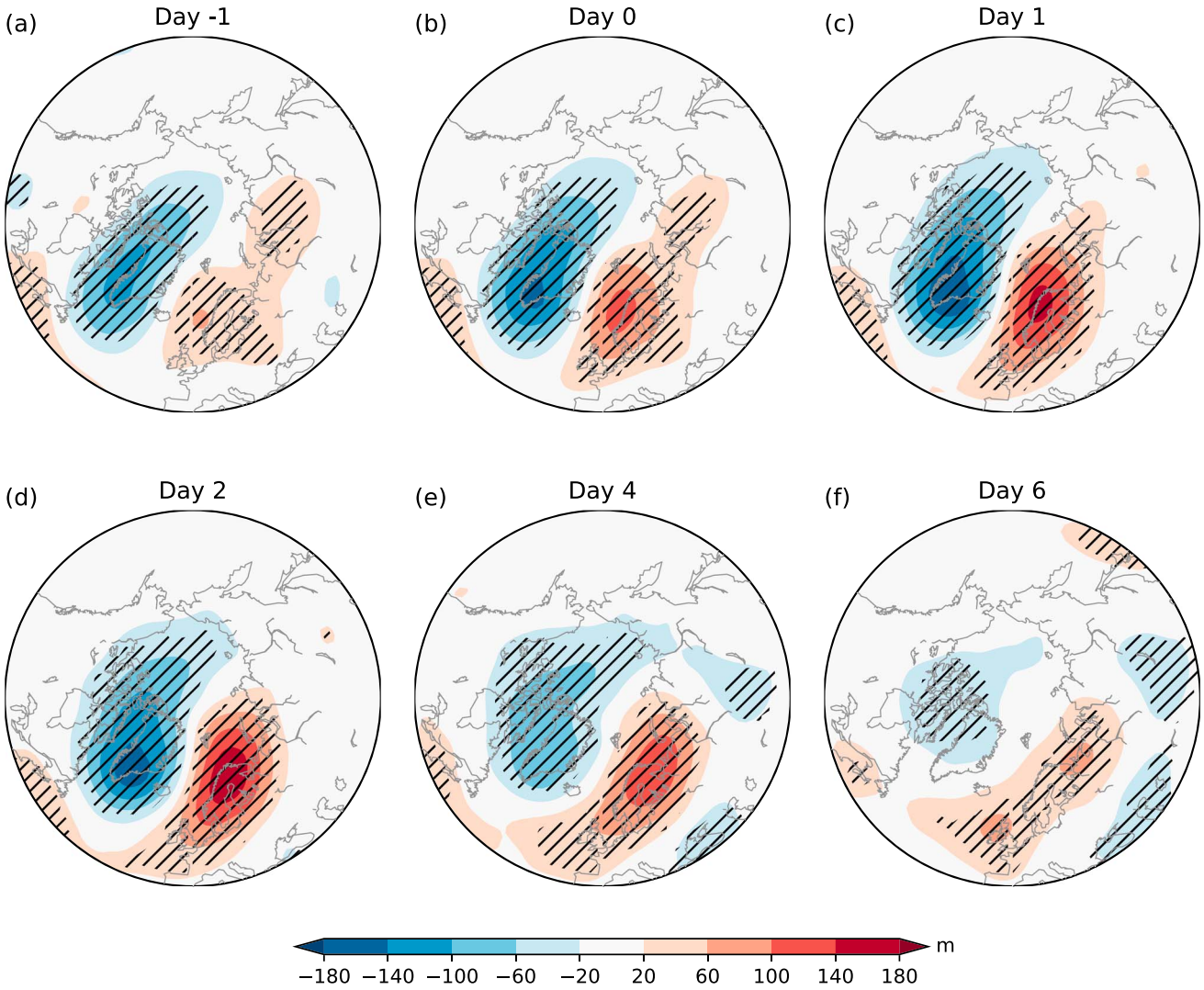

Figure 8. Same as Figure 6 except for the composites of Z500.

(Figure 6d), there is also significant cooling over the Eurasian continent interior. The lag composites of surface air temperature are also different from those of SIC tendency in impact duration: the impact of extreme moisture transport lasts much longer on the surface air temperature. There is still significant anomalous warming over the Barents-Kara Seas and the nearby coastal areas (Figure 6f) on lag day 14. Therefore, the duration of impact on the surface air temperature is at least 2 weeks, compared to the near 1 week duration of impact on the SIC tendency. This might be attributed to the effect of sea ice feedback: SIC reduction could induce more air-sea heat exchange, which continues to warm the surface air even after the extreme event has ended.

Extreme moisture transport events can impact SIC both dynamically and thermodynamically. The former effect involves sea ice drift induced by surface wind anomaly accompanied by extreme moisture transport, which is potentially important over the ice-export areas east of Greenland. In this study, however, we will only focus on the thermodynamical effect: enhanced downward longwave radiation at the surface. Figure 7 shows the impact of the extreme moisture transport on the surface downward longwave radiation. It is generally consistent with the SIC tendency patterns in Figure 5 and a similar tripole pattern as the surface air temperature in Figure 6. The duration of impact on the longwave radiation is similar to the SIC tendency and much shorter than the surface air temperature.

3.4. North Atlantic Weather Regimes

Figure 8 shows lag composites of the 500 hPa geopotential height (Z500), which helps identify weather regimes associated with the extreme moisture transport. The lag composites are dominated by a dipole

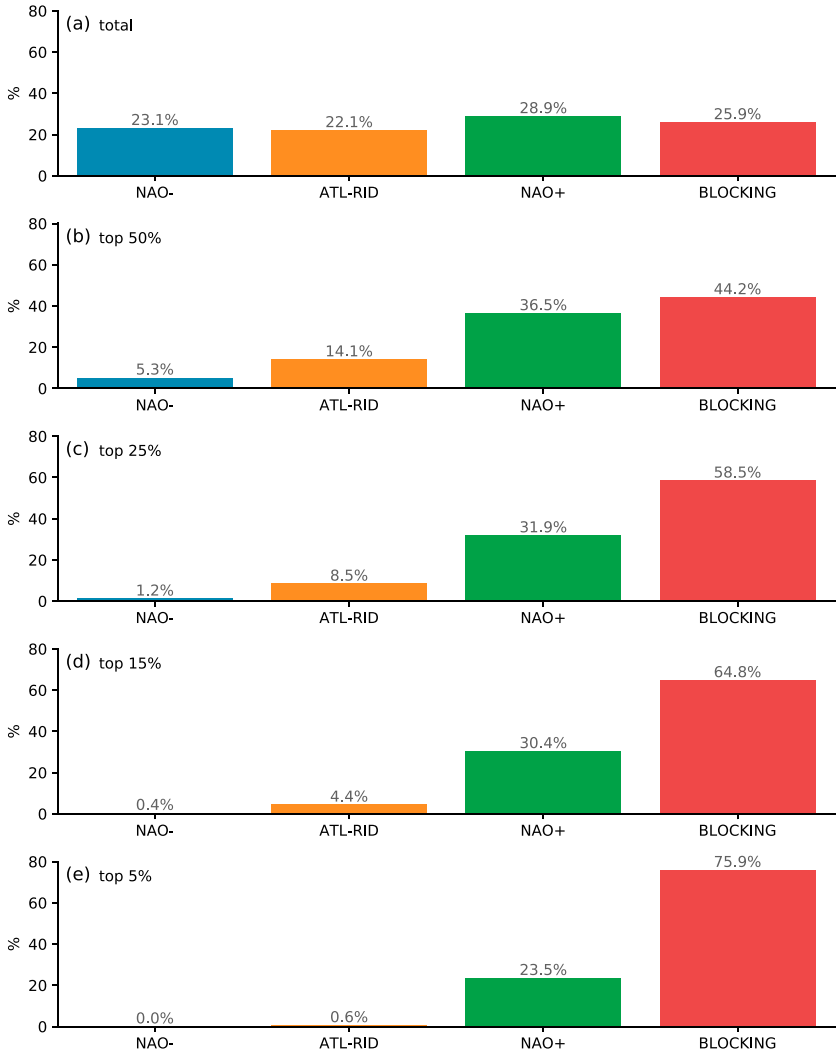

Figure 9. (a) North Atlantic daily weather regime histograms (normalized) in MAM of 1979–2014. The following subfigures are the same as Figure 9a except for days of Atlantic-VIqv70N greater than its (b) 50th, (c) 75th, (d) 85th, and (e) 95th percentiles.

pattern between an anomalous low centered over Greenland and an anomalous high centered over Scandinavia. A weak but significant anomalous high also appears to the east of Canada and weakly connects to the Scandinavia high. The Z500 patterns are resemble those in *Serreze et al.* [2015], which are defined in terms of extreme precipitation over Svalbard only. Comparing the dominating weather regimes over the Atlantic (Figure S1) to the composite Z500 field suggests that the extreme moisture transport is most associated with Figures S1a and S1b, or the blocking and positive phase NAO regimes.

Figure 9a shows the frequency of occurrence for the four weather regimes over the North Atlantic region during the MAM season. In general, the four weather regimes are evenly distributed. The difference between the highest (NAO^+) and lowest (Atlantic Ridge) frequency is only 6.8%. However, if we select days when the Atlantic-VIqv70N is greater than its median, the distribution is substantially modified (Figure 9b). The blocking regime stands out as the highest-frequency regime, which occupies 44.2% of the total days. The frequency of NAO^+ also increases to 36.5%, but it now ranks the second. A significant decrease occurs on the NAO^-, now to the lowest rank and only occupying 5.3% of total days. The increase of fraction of the blocking regime and the decrease of the NAO^- regime continue as we consider more and more extreme days of the Atlantic-VIqv70N. When it comes to the top 15% extremes, which is the focus in this study, the blocking occupies 64.8%, while the NAO^- takes only less than 1%.

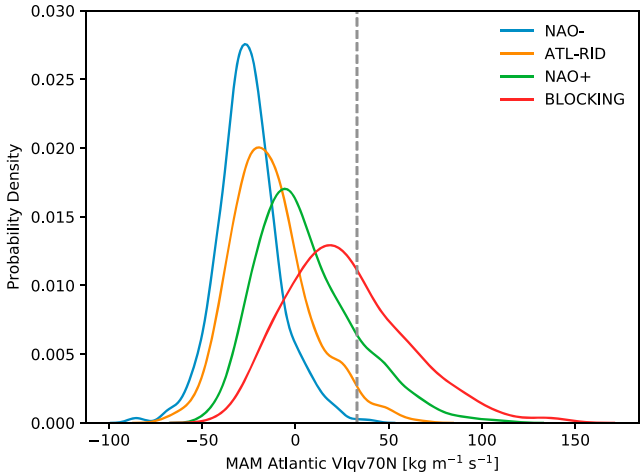

Figure 10. Probability density function (PDF) of Atlantic-VIqv70N for each of the four North Atlantic weather regimes. The vertical dashed line shows the 85th percentile of all the MAM Atlantic-VIqv70N daily values.

The relationship between the moisture transport into the Arctic and the North Atlantic weather regime can also be seen from the daily moisture transport anomaly PDF as shown in Figure 10. For the NAO$^-$ regime, the majority of the daily moisture transport anomaly is southward. The moisture transport anomaly that is greater than the threshold of 85th percentile is hardly seen for the NAO$^-$ regime. In contrast, more than half of the blocking regime days have a poleward moisture transport anomaly, and a significant portion of the days have a transport greater than the threshold of 85th percentile. The NAO$^+$ and Atlantic Ridge regimes are sitting between the two extremes, and the NAO$^+$ PDF profile is a little more toward the positive direction than that of the Atlantic Ridge regime. All these features are consistent with Figure 9 and indicate the dominance of the blocking regime in the extreme poleward moisture transport.

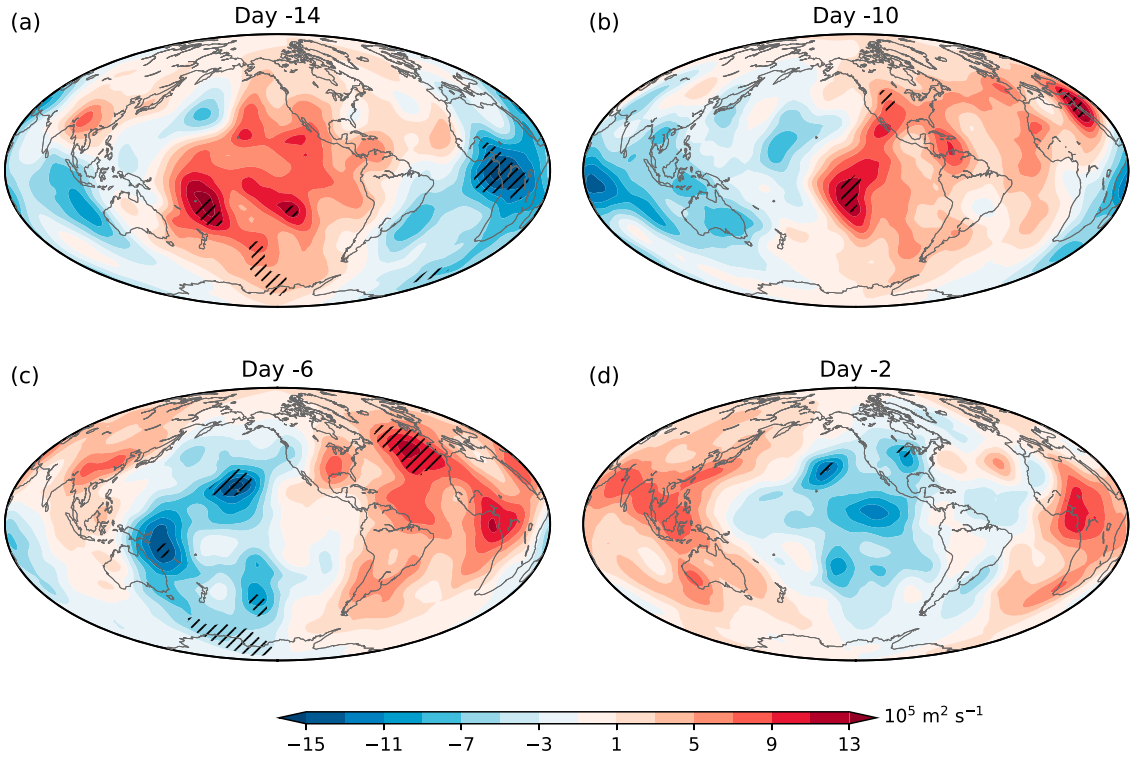

Figure 11. Same as Figure 6 except for the composites of 200 hPa velocity potential and lag days of −14, −10, −6, and −2. Centers of negative values indicate divergence in the upper troposphere and thus imply areas of active convection in the tropics.

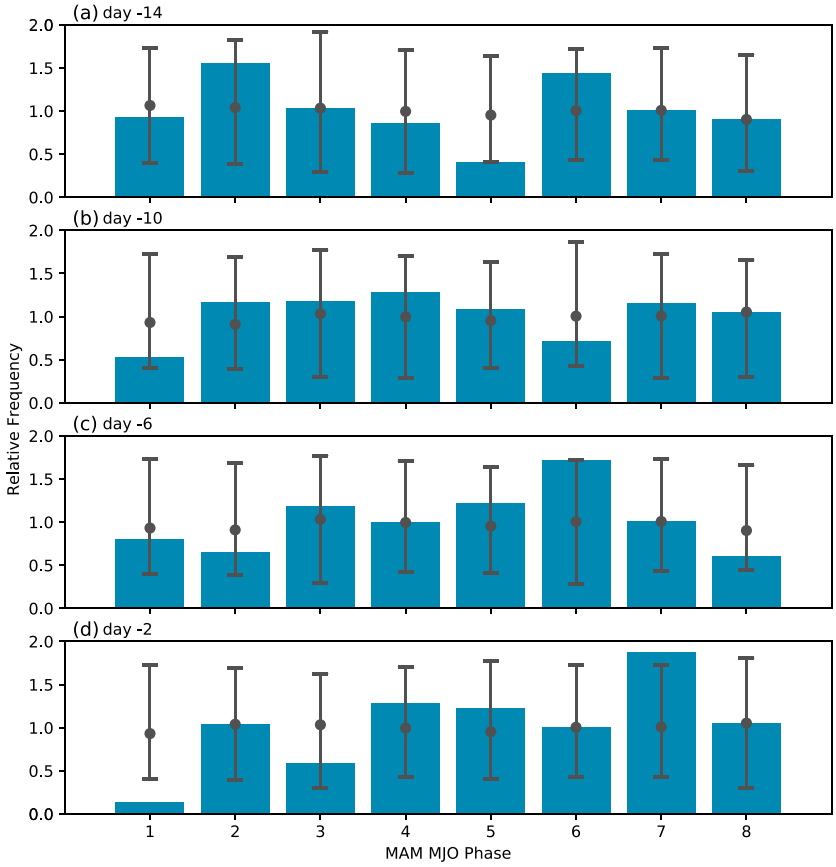

Figure 12. Distribution of MJO phases on lag day (a) −14, (b) −10, (c) −6, and (d) −2 of the extreme Atlantic-VIqv70N event in the MAM season (blue rectangles). The *y* axes are the relative frequency, i.e., the ratio of the actual frequency to the climatological frequency. The gray dots and error-bar-type lines show the medians and 95% confidence intervals estimated using a Bootstrap method.

3.5. Precursors From Tropical Convective Activity

Park et al. [2015a] concluded that extreme surface downward longwave radiation events and the associated moisture transport into the Arctic are preceded by anomalously high convective activity around the Maritime Continent by around 2 weeks. According to their hypothesis, the tropical convective forcing induces an atmospheric circulation anomaly that propagates poleward and can increase moisture transport into the Arctic 2 weeks later. This tropical-origin mechanism of anomalous moisture transport into the Arctic follows the tropics-extratropics interaction theory proposed by *Lee et al.* [2011]. Here we will test its validity for extreme moisture transport into the Arctic in spring.

Figure 11 shows the lag composites of MAM 200 hPa velocity potential (VP200). On lag day −14, the global VP200 pattern is dominated by negative values over tropical Africa and the Indian Ocean and positive values over the tropical Pacific Ocean. However, the values are generally insignificant. The most noticeable significant values are over tropical Africa, where the values are negative, indicating an upper troposphere divergence and enhanced convective activity over this region. Significant positive values are found over the South Pacific Convergence Zone (SPCZ) region, suggesting suppressed SPCZ activity. On lag day −10, the upper level divergence center moves to the Indian Ocean. However, the negative values of VP200 are not significant. In addition, the significant positive center also moves eastward to the east extreme of the SPCZ and suppresses convective activity there. On lag day −6, upper troposphere divergence occurs over the western Pacific Ocean and a small portion of the VP200 negative areas are significant. On lag day −2, the upper troposphere divergence moves eastward to the central and eastern Pacific Ocean. However, no significant negative values are found over the tropics. To summarize, the tropical convective precursive signal propagates eastward indicative of a possible role of the MJO [*Cassou*, 2008]. We therefore examine the MJO signal associated with extreme moisture transport into the Arctic.

Figure 12 shows histograms of MJO phase in MAM. The *y* axes show the relative frequency, which is defined as the ratio of the frequency for the lag days of the extreme Atlantic-VIqv70N events to the climatological frequency in the MAM season. The gray dots and error-bar-type lines show the median and 95 confidence interval estimated by a Bootstrap method. The blue rectangles show the actual values of the relative frequency and are considered as significant if they are out of the 95 confidence interval. On lag day −14, phases 2 and 6 have much higher frequency than their climatology but the values are not significant. Interestingly, phase 5 has a marginally significant low frequency. On lag day −10, the mode in the histograms seems to move rightward. However, no significant values are found. On lag day −6, a marginally significant high frequency is found for phase 6, which is consistent with the VP200 lag composite in Figure 11c. On lag day −2, another significant high frequency is found for phase 7, consistent with the VP200 lag composite in Figure 11d, although the VP200 values are not significant. At the same time, there is also a significant low frequency found for phase 1, which is consistent with positive VP200 values over the tropical Africa in Figure 11d. Again, the VP200 values are not significant there. Overall, there are some indications that springtime extreme moisture transport into the Arctic through Atlantic longitudes is preceded by large-scale, eastward propagating tropical convective activity, reminiscent of MJOs but somewhat faster. However, the signal-to-noise ratio is generally too low to be significant in the limited time range of observations.

4. Conclusions

The Arctic sea ice concentration (SIC) has been declining in recent decades accompanied by the Arctic Amplification (AA), yet its interannual variability is substantial and needs to be examined. It is hypothesized that extreme moisture transport into the Arctic, which brings both intense surface winds and a sudden increase of moisture, plays an important role in the Arctic SIC variability. Inspired by earlier studies [e.g., *Kapsch et al.*, 2013] as well as our analysis showing that spring moisture transport is crucial to the sea ice extend in the late summer and early fall, we focus on the character of extreme moisture transport in the spring season, i.e., March–May (MAM). Our interest is also focused on the moisture transport through the Atlantic sector, since the transport is dominant there compared to other longitudes, and it is also well correlated with the spring Arctic SIC variability.

Based on the time series of moisture transport into the Arctic through the Atlantic sector (Atlantic-VIqv70N), we find 58 extreme events with different durations during MAM over the years 1979–2014. Lag composite analysis based on these extreme events shows that extreme moisture transport events in MAM are indeed associated with sea ice reduction over the Greenland-Barents-Kara Seas. The impact duration is around 1 week. The extreme moisture transport events are also well correlated with Arctic surface air temperature with a longer-lasting anomaly in surface temperature for 2 weeks. The anomalous temperature shows a tripole pattern: anomalously warm over the Greenland-Barents-Kara Seas and cold to the west of Greenland and over the Eurasian continent interior. The cold anomaly over Eurasia that is strong a full week following the extreme event (Figure 6e) may also be associated with the teleconnection pattern found to be robust in a number of modeling studies in winter [e.g., *Honda et al.*, 2009; *Petoukhov and Semenov*, 2010]. Reduced sea ice concentration in the Barents and Kara Seas is found to lead to an intensified Siberian high and cold temperatures over the continent.

The blocking weather regime over the North Atlantic, which occupies more than 60% of the total extreme days, is mainly responsible for the extreme moisture transport into the Arctic. The NAO^- regime is rarely observed during the extreme days, with the frequency less than 1%. It has been hypothesized that large-scale tropical forcings precede the Arctic moisture transport by approximately 2 weeks. Indeed, we find an eastward propagating tropical convective signal, but our analysis shows that the link is weak and generally insignificant or marginally significant.

Acknowledgments
We thank Yannick Peings for helpful discussion on the application of the k-means clustering method on identification of the North Atlantic daily weather regimes. We also thank the three anonymous reviewers for their helpful and constructive comments. This research was supported by NOAA grant NA15OAR4310164. All the data used in this study are available to the public, and detailed descriptions can be found in the citations given in section 2.1.

References

Årthun, M., T. Eldevik, L. H. Smedsrud, Ø. Skagseth, and R. B. Ingvaldsen (2012), Quantifying the influence of Atlantic heat on Barents Sea ice variability and retreat, *J. Clim.*, *25*(13), 4736–4743, doi:10.1175/JCLI-D-11-00466.1.

Cassou, C. (2008), Intraseasonal interaction between the Madden–Julian oscillation and the North Atlantic oscillation, *Nature*, *455*(7212), 523–527, doi:10.1038/nature07286.

Dee, D. P., et al. (2011), The ERA-Interim reanalysis: Configuration and performance of the data assimilation system, *Q. J. R. Meteorol. Soc.*, *137*(656), 553–597, doi:10.1002/qj.828.

Ding, Q., et al. (2017), Influence of high-latitude atmospheric circulation changes on summertime Arctic sea ice, *Nat. Clim. Change*, *7*, 289–295, doi:10.1038/nclimate3241.

Graversen, R. G., and M. Burtu (2016), Arctic amplification enhanced by latent energy transport of atmospheric planetary waves, *Q. J. R. Meteorol. Soc.*, *142*(698), 2046–2054, doi:10.1002/qj.2802.
Graversen, R. G., T. Mauritsen, S. Drijfhout, M. Tjernström, and S. Mårtensson (2011), Warm winds from the Pacific caused extensive Arctic sea-ice melt in summer 2007, *Clim. Dyn.*, *36*(11), 2103–2112, doi:10.1007/s00382-010-0809-z.
Honda, M., J. Inoue, and S. Yamane (2009), Influence of low Arctic sea-ice minima on anomalously cold Eurasian winters, *Geophys. Res. Lett.*, *36*, L08707, doi:10.1029/2008GL037079.
Jakobson, E., T. Vihma, T. Palo, L. Jakobson, H. Keernik, and J. Jaagus (2012), Validation of atmospheric reanalyses over the central Arctic Ocean, *Geophys. Res. Lett.*, *39*, L10802, doi:10.1029/2012GL051591.
Kapsch, M.-L., R. G. Graversen, and M. Tjernstrom (2013), Springtime atmospheric energy transport and the control of Arctic summer sea-ice extent, *Nat. Clim. Change*, *3*(8), 744–748.
Koenigk, T., L. Brodeau, R. G. Graversen, J. Karlsson, G. Svensson, M. Tjernström, U. Willén, and K. Wyser (2013), Arctic climate change in 21st century CMIP5 simulations with EC-Earth, *Clim. Dyn.*, *40*(11), 2719–2743, doi:10.1007/s00382-012-1505-y.
Lee, S., T. Gong, N. Johnson, S. B. Feldstein, and D. Pollard (2011), On the possible link between tropical convection and the Northern Hemisphere Arctic surface air temperature change between 1958 and 2001, *J. Clim.*, *24*(16), 4350–4367, doi:10.1175/2011JCLI4003.1.
Michelangeli, P.-A., R. Vautard, and B. Legras (1995), Weather regimes: Recurrence and quasi stationarity, *J. Atmos. Sci.*, *52*(8), 1237–1256, doi:10.1175/1520-0469(1995)052<1237:WRRAQS>2.0.CO;2.
Mortin, J., G. Svensson, R. G. Graversen, M.-L. Kapsch, J. C. Stroeve, and L. N. Boisvert (2016), Melt onset over Arctic sea ice controlled by atmospheric moisture transport, *Geophys. Res. Lett.*, *43*, 6636–6642, doi:10.1002/2016GL069330.
Ogi, M., and J. M. Wallace (2007), Summer minimum Arctic sea ice extent and the associated summer atmospheric circulation, *Geophys. Res. Lett.*, *34*, L12705, doi:10.1029/2007GL029897.
Park, H.-S., S. Lee, S.-W. Son, S. B. Feldstein, and Y. Kosaka (2015a), The impact of poleward moisture and sensible heat flux on Arctic winter sea ice variability, *J. Clim.*, *28*(13), 5030–5040, doi:10.1175/JCLI-D-15-0074.1.
Park, H.-S., S. Lee, Y. Kosaka, S.-W. Son, and S.-W. Kim (2015b), The impact of Arctic winter infrared radiation on early summer sea ice, *J. Clim.*, *28*(15), 6281–6296, doi:10.1175/JCLI-D-14-00773.1.
Peings, Y., and G. Magnusdottir (2014), Forcing of the wintertime atmospheric circulation by the multidecadal fluctuations of the North Atlantic Ocean, *Environ. Res. Lett.*, *9*(3), 034018, doi:10.1088/1748-9326/9/3/034018.
Persson, P. O. G., M. D. Shupe, D. Perovich, and A. Solomon (2016), Linking atmospheric synoptic transport, cloud phase, surface energy fluxes, and sea-ice growth: Observations of midwinter SHEBA conditions, *Clim. Dyn.*,1–24, doi:10.1007/s00382-016-3383-1.
Petoukhov, V., and V. A. Semenov (2010), A link between reduced Barents-Kara sea ice and cold winter extremes over northern continents, *J. Geophys. Res.*, *115*, D21111, doi:10.1029/2009JD013568.
Pithan, F., and T. Mauritsen (2014), Arctic amplification dominated by temperature feedbacks in contemporary climate models, *Nat. Geosci.*, *7*(3), 181–184, doi:10.1038/ngeo2071.
Rigor, I. G., J. M. Wallace, and R. L. Colony (2002), Response of sea ice to the Arctic Oscillation, *J. Clim.*, *15*(18), 2648–2663, doi:10.1175/1520-0442(2002)015<2648:ROSITT>2.0.CO;2.
Serreze, M. C., and R. G. Barry (2011), Processes and impacts of Arctic amplification: A research synthesis, *Global Planet. Change*, *77*(1–2), 85–96, doi:10.1016/j.gloplacha.2011.03.004.
Serreze, M. C., A. D. Crawford, and A. P. Barrett (2015), Extreme daily precipitation events at Spitsbergen, an Arctic island, *Int. J. Climatol.*, *35*(15), 4574–4588, doi:10.1002/joc.4308.
Swift, C. T., and D. J. Cavalieri (1985), Passive microwave remote sensing for sea ice research, *Eos Trans. AGU*, *66*(49), 1210–1212, doi:10.1029/EO066i049p01210.
Tjernström, M., et al. (2015), Warm-air advection, air mass transformation and fog causes rapid ice melt, *Geophys. Res. Lett.*, *42*, 5594–5602, doi:10.1002/2015GL064373.
Walsh, J. E. (2014), Intensified warming of the Arctic: Causes and impacts on middle latitudes, *Global Planet. Change*, *117*, 52–63, doi:10.1016/j.gloplacha.2014.03.003.
Wheeler, M. C., and H. H. Hendon (2004), An all-season real-time multivariate MJO index: Development of an index for monitoring and prediction, *Mon. Weather Rev.*, *132*(8), 1917–1932, doi:10.1175/1520-0493(2004)132<1917:AARMMI>2.0.CO;2.
Winton, M. (2006), Amplified Arctic climate change: What does surface albedo feedback have to do with it?, *Geophys. Res. Lett.*, *33*, L03701, doi:10.1029/2005GL025244.
Woods, C., and R. Caballero (2016), The role of moist intrusions in winter Arctic warming and sea ice decline, *J. Clim.*, *29*(12), 4473–4485, doi:10.1175/JCLI-D-15-0773.1.
Woods, C., R. Caballero, and G. Svensson (2013), Large-scale circulation associated with moisture intrusions into the Arctic during winter, *Geophys. Res. Lett.*, *40*, 4717–4721, doi:10.1002/grl.50912.
Yang, W., and G. Magnusdottir (2016), Interannual signature in daily ITCZ states in the east Pacific in boreal spring, *J. Clim.*, *29*, 8013–8025, doi:10.1175/JCLI-D-16-0395.1.
Zhang, Y., W. Maslowski, and A. J. Semtner (1999), Impact of mesoscale ocean currents on sea ice in high-resolution Arctic ice and ocean simulations, *J. Geophys. Res.*, *104*(C8), 18,409–18,429, doi:10.1029/1999JC900158.